Spectral Properties of High-Power Distributed Bragg Reflector Lasers

Martin Achtenhagen, Nuditha Vibhavie Amarasinghe, Linglin Jiang, Jeffrey Threadgill, and Preston Young

Abstract—**In this paper, spectral data of distributed Bragg reflector lasers emitting around 974 nm and 1084 nm are presented. The devices are fabricated by a single-growth molecular beam epitaxy step, and the gratings are defined by holographic interferometry. Spectral dependencies on the grating and gain section lengths are systematically investigated in the so-called cleaved-back experiments. Experimental data for the side-mode suppression ratio, mode spacing, and group refractive index are given for devices emitting around 974 nm. In addition, the coupling efficiency between the grating and gain section is derived experimentally for devices emitting around 1084 nm.**

Index Terms—**Distributed Bragg reflector, laser diode, semiconductor lasers.**

I. Introduction

HIGH-POWER distributed Bragg reflector (DBR) lasers are used in numerous applications requiring single-frequency and wavelength tunability over a few tenths of a nanometer. Typical applications are Raman and absorption spectroscopy [1], narrow-line seeding and pumping of rare-earth-doped amplifiers [2], short-pulse generation [3], [4], terahertz generation, and generation of visible light by harmonic frequency conversion [5], [6]. The ability to fabricate these devices in a single epitaxial growth step with gratings defined by holographic interferometry significantly reduces the device complexity and processing time, thus minimizing manufacturing costs.

The spectral properties of DBR lasers are of major importance to the earlier mentioned applications, and the spectral requirements often vary significantly from one specific application to another. Therefore, proper understanding of the interplay between the DBR and the laser gain sections is a critical requirement for the overall device design.

In this paper, we systematically investigate the physical properties of the DBR laser grating and gain sections to study the impact on the emission spectra and the device performance. For this purpose, we selected two different well-characterized DBR laser structures---one series emitting around 974 nm and the second operating around 1084 nm. The presented results are by no means limited to these specific wavelengths and may serve as guidelines for design and operation of lasers at other wavelengths.

The paper is organized as follows. In Section II, we briefly highlight the manufacturing steps of the DBR laser diodes used in this work. Section III describes the systematic investigation of dependencies of the laser gain section length on the spectral properties for DBR devices emitting around 974 nm. Section IV presents analysis of the spectral characteristics due to variation of DBR reflectivity for devices emitting around 1084 nm. The summary of our results is given in Section V.

Manuscript received February 22, 2008; revised June 16, 2008 and September 05, 2008. First published Month 00, 0000; current version published nulldate. This work was supported in part by the NSF SBIR Phase II Grant 0450560.

The authors are with the Photodigm Inc., Richardson, TX 75081 USA (e-mail: machtenhagen@photodigm.com; vamarasinghe@photodigm.com; ljiang@photodigm.com; jthreadgill@photodigm.com; pyoung@photodigm.com).

Digital Object Identifier 10.1109/JLT.2008.2005848

II. DBR Laser Fabrication

DBR laser operating characteristics are extremely sensitive to variation in the physical parameters of both the starting wafer layer structure and in repeatable process control during the subsequent fabrication steps. Often, tolerance variations greater than 1%--2% can render the resulting lasers unsuitable for the intended design application. The laser structures used in this work are grown using molecular beam epitaxy (MBE) similar to the AlGaAs/GaAs wafer structures detailed in [7]. Prior to processing, photoluminescence mapping is performed to determine the exact material layer composition (aluminum mole fraction) and the uniformity across each wafer. The values obtained are then averaged and used for tailored design of the required gain ridge, DBR grating parameters (period, profile, and etch depth), as well as critical process parameters required during subsequent fabrication steps.

Photolithographic processing utilizes multiple mask layouts for metal and dielectric depositions, as well as intermediate etch processes throughout the laser device fabrication. Basic alignment and exposures are done using a Karl Suss MJB3 mask aligner with I-line operating wavelength around 365 nm. The ridge mask is used to pattern nominal 3-μm-wide stripes defining the ridge waveguides for the laser gain sections. Pattern transferal is accomplished by wet etching in a standard $H_2SO_4 : H_2O_2 : H_2O$ solution with specific ratios determined by the material composition and the designed target etched depth and profile. The average etch rate monitored during etching is $\sim$ 1600 Å/min. After etching the top wafer layers, the resist thickness is measured along with the etch step to verify the final ridge depth (typically around 1.2 μm).

Following the wet etch steps, a dielectric layer along with Ti/Pt/Au p-contact metal layers are deposited along the gain ridge section. The dielectric is deposited using plasma-enhanced chemical vapor deposition from silane and nitrogen precursors at a deposition temperature near 150°C. The Ti and Pt are deposited at very slow rates to minimize the tensile stress in the metal contacts. Liftoff is accomplished by substrate immersion

0733-8724/$25.00 © 2009 IEEE

IEEE Proof

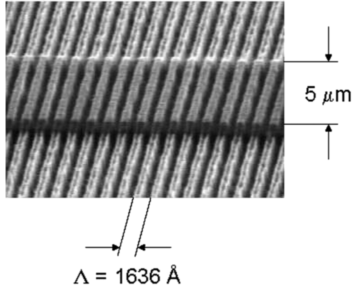

Fig. 1. SEM image of the DBR grating. As indicated, the grating period is about $\Lambda = 1636$ Å and the width of the grating confinement ridge is about 5 μm.

in an acetone bath for 5 min, followed by an acetone spray wash. Three annealing steps are also performed throughout the process. The first two steps reduce the stress between the deposited metal and dielectric layers, and the final step is performed to anneal the n-contact metal to the substrate.

Gratings are fabricated using a holographic interferometry process. The interference pattern is created using a single-beam Lloyd's mirror setup similar to that described in [8]. A frequency-doubled argon laser with an emission wavelength of $\lambda = 244$ nm and an output power of 40 mW is used to expose the photoresist. The laser is operated in a single-spatial mode, and an intracavity etalon (temperature-stabilized 1-cm-thick fused silica with a corresponding free spectral range of 10 GHz) is used to insure single-longitudinal mode operation. The Lloyd's mirror has a 628 nm optical flatness of $\lambda/20$ and is coated to yield a maximum reflectivity for a wide range of angles corresponding to different grating periods at the 244 nm exposure wavelength. The grating period is controlled using a rotating stage assembly containing both the mirror and an adjustable substrate holder. The grating period for a device with an emission wavelength at 1084 nm is calculated to be 1636 Å assuming an effective waveguide refractive index of 3.313, and the corresponding period for a device emitting at 974 nm is calculated to be 1463 Å with an estimated effective index around 3.329.

The photoresist grating is then dry etched in a reactive ion etcher with a $SiCl_4 : CH_4/H_2 : Ar$ plasma. The chamber power and pressure are adjusted to provide an etch selectivity around 1:4 between photoresist and substrate material. The target grating etch depth for the devices in this work is approximately 1300 Å, with a grating duty cycle prior to development of 50%. In practice, it is found that the etch rate is inversely proportional to the grating duty cycle. After the DBR gratings are etched, a 5-μm-wide confinement ridge is defined and transfer etched onto each grating section as shown in Fig. 1.

Following fabrication of the confinement ridge, an additional layer of Si_3N_4 is deposited to serve as a protective film over the gratings. Final processing includes wafer thinning to 100 μm, polishing, and n-contact metallization. For the devices in this work, no antireflection (AR) coatings are deposited on the cleaved laser facets; thus, the maximum output power from these devices is substantially reduced. With appropriate front facet AR coatings, the slope efficiency for the 974-nm devices is typically around 0.72 W/A with a maximum output power around 425 mW. AR-coated devices emitting near 1084 nm have a typical slope efficiency of 0.85 W/A and maximum power around 550 mW.

TABLE I
MEASURED VALUES OF THE MODE SPACING FOR DIFFERENT GAIN LENGTHS. THE EFFECTIVE DBR LENGTH IS AROUND 95 μm AND THE EMISSION WAVELENGTH IS AROUND 974 nm

Gain Length L_{gain} (μm)	**Mode Spacing δλ (Å)**
600	1.46 ± 0.08
900	1.05 ± 0.07
1200	0.76 ± 0.05
1500	0.61 ± 0.06

III. CHARACTERISTICS OF 974-nm DBR LASERS

In general, a DBR laser diode is capable of emitting in a single spectral mode over a wide operating range. This mode has usually a wavelength closest to the DBR peak reflectivity, and hence requires the lowest amount of gain to reach threshold. With increasing injection current, the device temperature increases and the cavity modes are shifted toward longer wavelengths. This shift of the cavity modes occurs at a faster rate than the shift in reflectivity spectrum. As a consequence, the lasing mode shifts away from the DBR peak reflectivity until an adjacent mode has a higher reflectivity. At this point, the emission wavelength jumps to the new cavity mode at a shorter wavelength.

The exact wavelength change depends on the cavity mode spacing, which itself depends on the effective cavity length and the group refractive index. The effective cavity length is the sum of the effective DBR length and the length of the gain section. The effective DBR length can directly be estimated by the following expression [9]:

$$L_{\mathrm{DBR,eff}} = \frac{1}{2\kappa}\tanh(\kappa L_{\mathrm{DBR}}) \quad (1)$$

where κ is the grating coupling coefficient and L_{DBR} is the physical grating length. The devices in this work are designed to have a target coupling coefficient $\kappa = 50\,\mathrm{cm}^{-1}$ and, if not stated otherwise, a grating length of 400 μm. Inserting these numbers into (1) yields an effective DBR length of ~ 95 μm.

To derive a numerical value for the group refractive index, the gain section is cleaved back from an initial length of 1500 μm down to 600 μm. The wavelength changes are measured and averaged over several jumps as presented in Table I. The group refractive index is found from a numerical fit to the linear relation between the inverse mode spacing and the gain length, i.e., $1/\delta\lambda = 2n_{g,\mathrm{eff}}(L_{\mathrm{gain}} + L_{\mathrm{DBR,eff}})/\lambda^2$ resulting in a value of $n_{g,\mathrm{eff}} = 4.895$.

With decreasing gain length, the device temperature increases considerably as indicated by the different slopes of the wavelength versus current curves shown in Fig. 2. Due to the presence

IEEE Proof

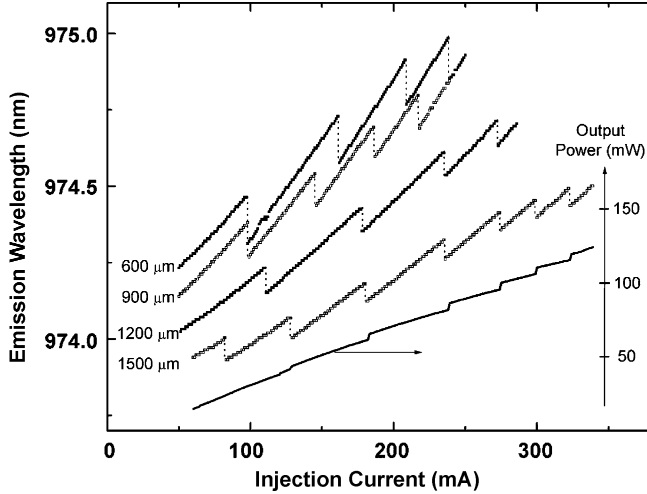

Fig. 2. Emission wavelength versus injection current for four different gain section lengths. The DBR length amounts to $L_{\rm DBR} = 400\,\mu{\rm m}$. The inset shows the output power against the injection current for the DBR laser with a gain section length of 1500 μm.

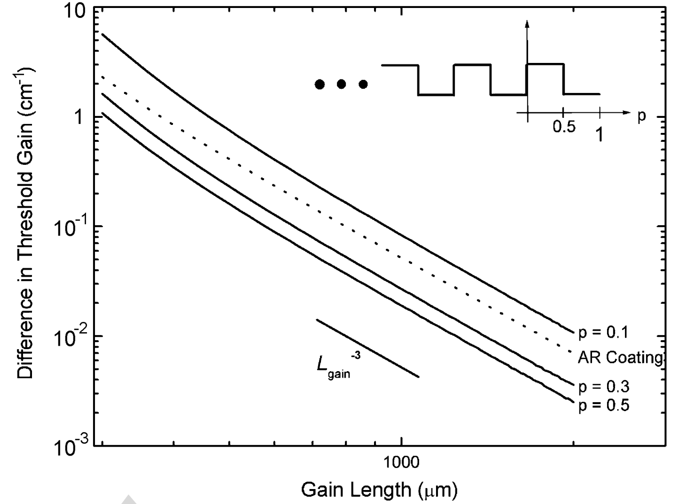

Fig. 3. Simulated threshold gain difference between lasing mode and closest side mode. The inset shows the definition of the *p*-value with respect to the grating period.

of spectral hole burning, each wavelength jump corresponds to a discontinuity in the device light-current (*L*--*I*) curve. The inset of Fig. 2 shows a reference *L*--*I* curve for the device with 1500-μm gain length. Note that the increasing discontinuity with increasing injection current may be attributed to the power dependency of the spectral hole-burning effect. For specific device designs, under high injection current operating conditions, the relative degree of spectral hole burning can cause the preferred lasing mode to jump to a wavelength spaced more than one cavity mode away from the initial lasing wavelength. In this work, device design and operating conditions were chosen to limit the wavelength jumps to occur into adjacent cavity modes.

The side-mode suppression ratio (SMSR) of a DBR laser diode depends not only on the grating and cavity design but also on spectral and spatial hole-burning effects. These secondary effects are neglected in the following evaluation. Additionally, the wavelength of the lasing mode is assumed to be aligned with the DBR peak reflectivity. The difference in the threshold gain between the lasing mode and the closest side mode can easily be derived using (1)

$$\Delta G = \frac{1}{2(L_{\rm gain} + L_{\rm DBR,eff})} \ln\left(\frac{R_{\rm DBR}(\lambda_1)}{R_{\rm DBR}(\lambda_0)}\right) \qquad (2)$$

where $R_{\rm DBR}(\lambda_{0,1})$ is the intensity reflectivity of the DBR grating at the lasing wavelength λ_0 and side-mode wavelength λ_1, respectively. Again, the coupling coefficient of the DBR grating is assumed to be $\kappa = 50\ {\rm cm}^{-1}$.

With increasing gain length, the threshold gain difference decreases rapidly. For a gain length larger than 500 μm, the threshold gain difference can be approximated by $\Delta G \sim 1/L^3_{\rm gain}$ (see Fig. 3). The phase of the residual reflection originating from the semiconductor to air interface at the DBR termination affects the overall reflectivity and depends on the exact location with respect to the grating period (see inset of Fig. 3) [10]. For this analysis, since multiple devices are analyzed, the exact locations were assumed randomly distributed for each individual device. Statistically, for most of the randomly cleaved devices ($p \sim 0.15 - 0.85$), the threshold gain difference is compared to be smaller than those devices with an AR facet coating. Only for devices with *p*-values close to $p \sim 0.1$ or $p \sim 0.9$, the threshold gain difference exceed the value from AR-coated devices (see Fig. 3). It should be noted that the peak reflectivity of the DBR is higher for *p*-values ranging from 0.2 to 0.8 and has its maximum value for $p = 0.5$.

The optical spectra for different power levels, i.e. injection currents, are shown in Fig. 4 for a device with gain length of 1500 μm. The device operates in a single-longitudinal mode with SMSR exceeding 45 dB for each of the given power levels. The resolution of the optical spectrum analyzer (ANDO AQ6317 OSA) was set to 0.1 Å, and the noise floor was below -90 dBm. Additional measurements were performed for gain lengths of 600, 900, and 1200 μm with the resulting SMSRs monitored as a function of injection current. Fig. 5 shows the SMSR curves for each cleaved device gain length.

The SMSR typically exceeds 45 dB over most of the range of current values. Note that the curves in Fig. 5 are offset for clarity. In the transition regions, where the emission wavelength jumps from the lasing mode to the closest neighboring mode, the SMSR decreases considerably. These drops in the SMSR also align with the wavelength changes and the corresponding output power discontinuities shown in Fig. 2. For low-level injection current between approximately 65 mA and 80 mA, the device with a gain length of 1500 μm shows a large range of current where the device actually emits in two longitudinal modes simultaneously. The SMSR in this region is below 10 dB.

The threshold gain difference between cavity modes for these 1500-μm devices at low injection current does not provide sufficient mode discrimination to allow lasing at a single wavelength. At higher power levels, spectral hole burning becomes significant and provides the necessary gain difference to favor selection of a single lasing mode [11]. The maximum SMSR

IEEE Proof

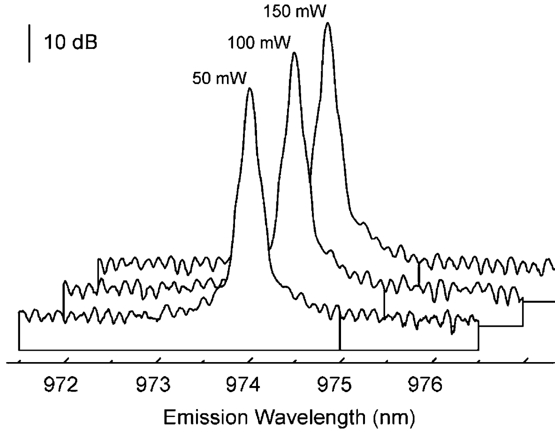

Fig. 4. Emission spectra at different power levels for a DBR laser with a gain section length of 1500 μm.

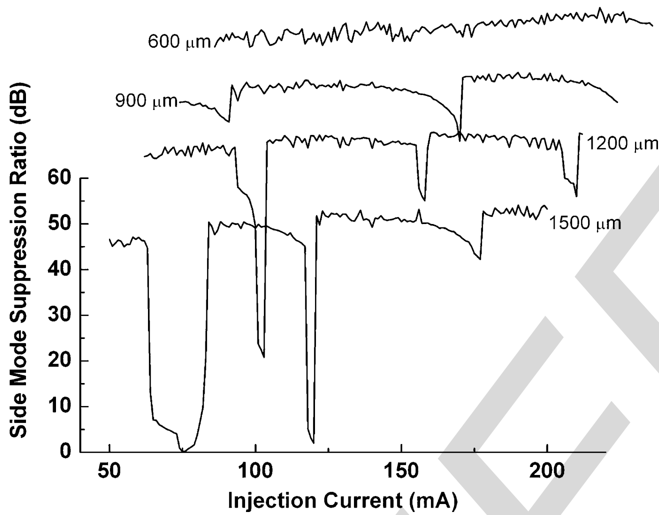

Fig. 5. Measured SMSR as a function of the injected laser current. The gain length varies from $L_{\mathrm{gain}} = 600$, 900, 1200, and 1500 μm. The DBR length for all devices is $L_{\mathrm{DBR}} = 400$ μm. The SMSR curves are individually offset for clarity by 10 dB in the vertical direction and 10 mA in the horizontal direction.

value slightly increases from approximately 45 dB for the long gain section devices to around 50 dB for shortest investigated gain lengths. For the 600-μm gain length devices, the SMSR appears roughly independent of the injection current and partly due to resolution of the OSA measurements, does not show a decline in SMSR immediately preceding a mode hop. The measurements show that for short-cavity length devices, the onset of lasing into an adjacent mode occurs very rapidly with increasing current as opposed to devices with longer gain sections.

IV. Characteristics of 1084-nm DBR Lasers

To derive an estimate of the DBR reflectivity, the back-to-front ratio of the slope efficiencies is monitored for different DBR lengths. For this series of devices, the DBR section is cleaved back from an initial length of 800 μm in steps of 100 μm until the laser back reflection consists of a single refractive index step, i.e. becomes a Fabry--Perot type laser. The data are collected and averaged from eight individual laser devices. The

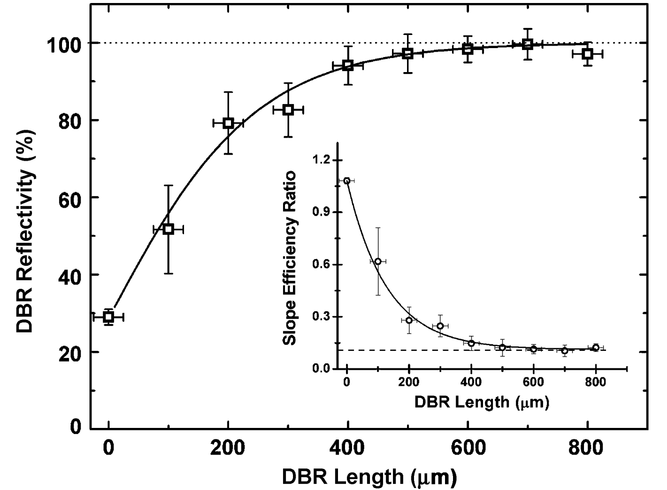

Fig. 6. Measured (points) and simulated (solid line) DBR reflectivity as a function of grating length. The inset shows the slope efficiency ratio between the back and front facet emission for increasing grating length. The asymptotic constant offset value represents a coupling efficiency of $\eta = 0.936$, which is considered in the derivation for the DBR reflectivity.

slope efficiency ratio of the back-to-front emission can be calculated using [12]

$$\frac{\eta_{\mathrm{DBR}}}{\eta_f} = \frac{\sqrt{R_f}(1 - R_{\mathrm{DBR}})}{\sqrt{R_{\mathrm{DBR}}}(1 - R_f)} \tag{3}$$

where the DBR is assumed to be located on the back side of the laser, and R_f and R_{DBR} are the intensity reflection coefficients of the front and DBR back facet, respectively. The optical coupling efficiency between the gain and DBR sections amounts to $\eta = 0.936$, which is derived from the asymptotic constant offset value indicated in the inset of Fig. 6. This value results from high-mode overlap between the gain and DBR sections and is optimized by appropriate choice of the ridge width in the different sections.

Equation (3) is used to derive the DBR reflectivity for the different grating lengths assuming the earlier derived coupling coefficient. The results are presented in Fig. 6. Note that the squared value of the coupling coefficient is used due to the back and forth propagation of the field between gain and DBR sections. With increasing DBR length, the reflectivity increases until it approaches its maximum value close to 100%. Fig. 6 also shows the DBR reflectivity calculated using the transmission matrix method. The effective refractive index amounts to $n_{\mathrm{eff}} = 3.32$ with an index modulation depth of $\Delta n = 2.7 \times 10^{-3}$ and a grating period of $\Lambda = 1636$ Å. These values corresponds to a coupling coefficient of $\kappa = 50$ cm^{-1}, which agrees well with the designed target value for the DBR grating (see solid line in Fig. 6). Also, it is noted that the error in the experimental data increases with shorter DBR length. Again, the residual reflection originating from the semiconductor to air interface at the DBR termination affects the overall reflectivity and depends on the exact location with respect to the grating period. The exact location, however, is randomly distributed for each individual device. It can easily be shown that for shorter DBR lengths, the

IEEE Proof

influence of the random cleave becomes larger and results in larger variations in the effective DBR reflectivity.

V. Summary

This paper has presented an experimental study of the spectral properties of DBR laser diodes emitting around 974 nm and 1084 nm. The investigated devices are grown in a single-step MBE process with gratings defined by holographic interferometry. They are capable of emission into a single lateral and longitudinal mode over a wide operation range.

The dependence of the mode spacing and the SMSR on the cavity design are systematically studied using devices emitting around 974 nm. For this purpose, several devices are measured with an initial gain length of 1500 μm and then the gain sections are shortened by cleaving-back in steps of 300 μm. A group refractive index of 4.895 is found, from which the mode spacing for any given gain ridge length can easily be derived. Further, it is found that the SMSR slightly increases with increasing mode spacing.

The effective DBR reflectivity, which is an important device parameter, is investigated using devices emitting around 1084 nm. To estimate the DBR reflectivity and the coupling efficiency, the grating sections are successively shortened and the slope efficiency ratio is monitored. A coupling efficiency between the DBR and gain section of $\eta = 0.936$ is found and corresponds well to the design DBR coupling coefficient of $\kappa = 50\ \mathrm{cm}^{-1}$. Finally, it is shown that the exact cleaving position and, therefore, the relative phase between the grating and the semiconductor--air interface significantly influences the exact value for the effective DBR reflectivity.

Acknowledgment

The authors thank R. Mangham, D. Phan, and P. Le for device processing.

References

[1] J. S. Major and D. F. Welch, "Singlemode InGaAs/GaAs distributed Bragg reflector laser diodes operating at 1083 nm," *Electron. Lett.*, vol. 29, no. 24, pp. 2121–2122, 1993.

[2] K. Fukagai, H. Chida, S. Ishikawa, H. Fujii, and K. Endo, "High-power 1.02 μm InGaAs/AlGaAs strained quantum well lasers with GaInP buried waveguides for pumping Pr^{3+}-doped optical amplifiers," *Electron. Lett.*, vol. 29, pp. 146–147, 1993.

[3] K.-H. Hasler, H. Wenzel, A. Klehr, and G. Ebert, "Simulation of the generation of high-power pulses in the GHz range with three-section DBR lasers," *Proc. Inst. Elect. Eng.—Optoelectron.*, vol. 149, no. 4, pp. 152–160, Aug. 2002.

[4] P. P. Vasil'ev, I. H. White, and M. J. Fice, "Narrow line high power picosecond pulse generation in a multicontact distributed feedback laser using modified Q switching," *Electron. Lett.*, vol. 29, pp. 561–563, 1993.

[5] K. A. McIntosh, E. R. Brown, K. B. Nichols, O. B. McMahon, W. F. DiNatale, and T. M. Lyszczarz, "Terahertz photomixing with diode lasers in low-temperature-grown GaAs," *Appl. Phys. Lett.*, vol. 67, no. 26, pp. 3844–3846, 1995.

[6] M. H. Hu, H. K. Nguyen, K. Song, Y. Li, N. J. Visovsky, X. Liu, N. Nishiyama, S. Coleman, L. C. Hughes, Jr., J. Gollier, W. Miller, R. Bhat, and C. Zah, "High-power high-modulation-speed 1060-nm DBR lasers for green-light emission," *IEEE Photon. Technol. Lett.*, vol. 18, no. 4, pp. 616–618, Feb. 2006.

[7] C. Harder, P. Buchmann, and H. Meier, "High-power ridge-waveguide AlGaAs GRIN-SCH laser diode," *Electron. Lett.*, vol. 22, no. 20, pp. 1081–1082, 1986.

[8] [Online]. Available: http://www.ece.byu.edu/photonics/holography.phtml

[9] L. A. Coldren and S. W. Corzine, *Diode Lasers and Photonic Integrated Circuits*. New York: Wiley, 1995.

[10] M. Achtenhagen, N. V. Amarasinghe, and G. A. Evans, "High-power distributed Bragg reflector lasers operating at 1065 nm," *Electron. Lett.*, vol. 43, no. 14, pp. 757–759, 2007.

[11] H. Kawanashi and P. E. Petersen, "Gain suppression in GaAs/AlGaAs TJS lasers," *IEEE J. Quantum Electron.*, vol. 17, no. 6, pp. 823–824, Jun. 1981.

[12] G. H. B. Thompson, *Physics of Semiconductor Laser Devices*. New York: Wiley, 1980.

Martin Achtenhagen received the Ph.D. degree in physics from the Swiss Federal Institute of Technology (EPFL), Lausanne, Switzerland, in 1996, for his work on gain-coupled DFB laser diodes.

After Postdoctoral work at the IBM Zurich Research Laboratory, Zurich, Switzerland, he became a Research Staff Member at IBM Zurich, in 1997, and was involved in work on quantum-well semiconductor lasers, with the emphasis on the design and characterization of high-power GaAs-based lasers. By ownership change, in 1997, he became a Research Staff Member of JDS Uniphase, Eatontown, NJ. In 1998, he was on leave for one year at Spectracom to develop a new generation of pump lasers for EDFA applications, and then returned to JDS Uniphase, where he managed the forward-looking group with emphasis on Raman and EDF amplifiers. In 2002, he became a Senior Research Associate at the Swiss Federal Institute of Technology (EPFL) and worked on the simulation of long-wavelength vertical-cavity surface-emitting laser diodes. In 2006, he joined Photodigm Inc. as Vice President of Engineering developing next generation of reliable high-power distributed feedback reflector lasers.

Dr. Achtenhagen serves as an Associate Editor of Optical Fiber Technology.

Nuditha Vibhavie Amarasinghe received the B.S. degree (with honors) in physics from University of Colombo, Sri Lanka, in 1993, and the M.S. degree in physics from Wichita State University, Wichita, KS, in 1998, and the Ph.D. degree in electrical engineering from Southern Methodist University, Dallas, TX, in 2001.

From 1993 to 1996, he served as an Academic Staff Member in the Department of Physics, University of Colombo. He joined Photodigm Inc., in 2001, and holds currently the position of Principal Lead Engineer. His research interests include the studies of first- and second-order gratings, DBRs and their impact on basic device properties, improvements on process of DBR lasers in production, manufacturability of lateral gratings with a holographic grating process, high power grating surface emitters, and laser packaging systems. He has authored or coauthored several journal publications and conference proceedings, a book chapter, and five patents.

Linglin Jiang received the M.S. degree in electrical engineering from New Mexico State University, Las Cruces, in 2000, and is currently working towards her Ph.D. degree in electrical engineering at Southern Methodist University, Dallas, TX.

In 2001, she joined The Photonics Group of Corning Cable Systems, Keller, TX, as a Product Engineer, where she focused on design and developing pigtail, collimator, and designed the test station for coupler characterization. Since 2007, she has been an Electrical Engineer at Photodigm Inc., Richardson, TX. Her research interests include epitaxial structure design of laser diodes for a wavelength range from 780 nm to 1550 nm, DBR laser design, laser fabrication, laser characterization, lens design for laser beam collimation, and quantum well intermixing.

Ms. Jiang is a member of the IEEE Photonics Society, Dallas Chapter.

Jeffrey Threadgill received the Associates of Applied Science degree in laser and electro-optics from Texas State Technical College, Waco, TX, in 2006.

He had been a Research Assistant for three semesters at the Center for Astrophysics, Apace Physics, and Engineering Research Facility (C.A.S.P.E.R.). C.A.S.P.E.R. is a joint facility put together by the Baylor Physics Department and TSTC Laser Department. His research interests include plasma physics and hypervelocity experiments. Currently, he is a Process Technician at Photodigm, Inc. Richardson, TX, and is also pursuing his engineering degree.

IEEE Proof

Preston Young received the Ph.D. degree in electrical engineering from the University of Texas, Arlington, in 2006.

He has over 15 years experience in the semiconductor manufacturing and electrical design engineering. He worked as an Electrical Design Engineer for multiple Texas area businesses. From 2007, he has been a Senior Electrical Engineer in charge of laser production test and measurement at Photodigm Inc., Richardson, TX. His research interests include design and fabrication of resonant optical and microwave waveguide grating structures. He was awarded a patent for development of laser devices incorporating these structures. He has authored and coauthored numerous papers in the field of optical semiconductor engineering.

He is a member of the IEEE and IEEE Photonics Society, in the Fort Worth Chapter, and also the Academy of Model Aeronautics.

IEEE Proof